Synthesis and electromagnetic wave absorption property of amorphous carbon nanotube networks on a 3D graphene aerogel/BaFe12O19 nanocomposite

Zhao, Tingkai; Ji, Xianglin; Jin, Wenbo; Xiong, Chuanyin; Ma, Wenxiu; Duan, Shichang; Dang, Alei; Li, Hao; Li, Tiehu; Shang, Songmin; Zhou, Zhongfu

Published in:
Journal of Alloys and Compounds

DOI:
10.1016/j.jallcom.2017.03.001

Publication date:
2017

Citation for published version (APA):
Zhao, T., Ji, X., Jin, W., Xiong, C., Ma, W., Duan, S., Dang, A., Li, H., Li, T., Shang, S., & Zhou, Z. (2017). Synthesis and electromagnetic wave absorption property of amorphous carbon nanotube networks on a 3D graphene aerogel/BaFe12O19 nanocomposite. *Journal of Alloys and Compounds*, *708*, 115-122. https://doi.org/10.1016/j.jallcom.2017.03.001

Accepted Manuscript

Synthesis and electromagnetic wave absorption property of amorphous carbon nanotube networks on a 3D graphene aerogel/$BaFe_{12}O_{19}$ nanocomposite

Tingkai Zhao, Xianglin Ji, Wenbo Jin, Chuanyin Xiong, Wenxiu Ma, Chuan Wang, Shichang Duan, Alei Dang, Hao Li, Tiehu Li, Songmin Shang, Zhongfu Zhou

PII: S0925-8388(17)30770-3

DOI: 10.1016/j.jallcom.2017.03.001

Reference: JALCOM 41039

To appear in: *Journal of Alloys and Compounds*

Received Date: 3 January 2017

Revised Date: 23 February 2017

Accepted Date: 1 March 2017

Please cite this article as: T. Zhao, X. Ji, W. Jin, C. Xiong, W. Ma, C. Wang, S. Duan, A. Dang, H. Li, T. Li, S. Shang, Z. Zhou, Synthesis and electromagnetic wave absorption property of amorphous carbon nanotube networks on a 3D graphene aerogel/$BaFe_{12}O_{19}$ nanocomposite, *Journal of Alloys and Compounds* (2017), doi: 10.1016/j.jallcom.2017.03.001.

Graphical abstracts

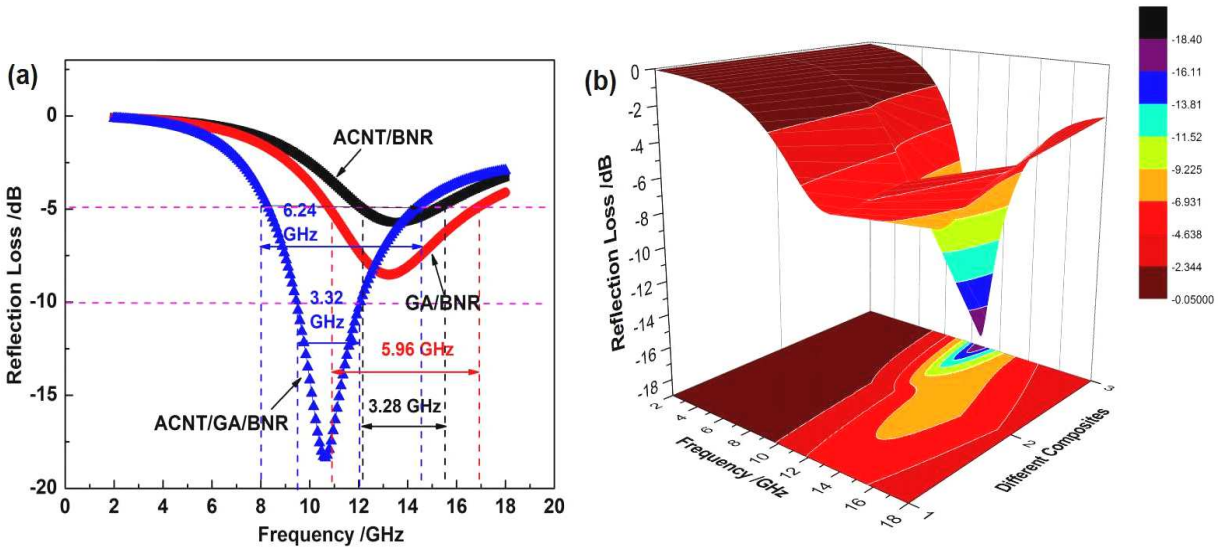

Synthesis and electromagnetic wave absorption property of amorphous carbon nanotube networks on a 3D graphene aerogel/$BaFe_{12}O_{19}$ nanocomposite

Tingkai Zhao[1,*], Xianglin Ji[1,*], Wenbo Jin[1], Chuanyin Xiong[1], Wenxiu Ma[1], Chuan Wang[1], Shichang Duan[1], Alei Dang[1], Hao Li[1], Tiehu Li[1], Songmin Shang[2], Zhongfu Zhou[3]

[1] *State Key Laboratory of Solidification Processing, Shaanxi Engineering Laboratory for Graphene New Carbon Materials and Applications, School of Materials Science and Engineering, Northwestern Polytechnical University, Xi'an 710072, China*

[2] *Institute of Textiles and Clothing, The Hong Kong Polytechnic University, Kowloon, Hong Kong*

[3] *Department of Physics, Aberystwyth University, Aberystwyth SY23 3FL, UK*

Abstract: Homogeneous amorphous carbon nanotube (ACNT) networks have been synthesized using floating catalyst chemical vapor deposition method on a 3D graphene aerogel (GA)/ $BaFe_{12}O_{19}$ (BF) nanocomposite which was prepared by a self-propagating combustion process. The as-synthesized ACNT/GA/BF nanocomposite with 3D network structures could be directly used as a good absorber material for electromagnetic wave absorption. The experimental results indicated that the minimum reflection loss of ACNT/GA/BF composite with a thickness of 2 mm was -18.35 dB at 10.64 GHz in the frequency range of 2-18 GHz. The frequency bandwidth of the reflection loss below -10 dB was 3.32 GHz and below -5 dB was 6.24 GHz, respectively. The 3D

[*] Corresponding author. E-mail address: ztk-xjtu@163.com (T.K. Zhao) and jixianglinnwpu@163.com (X.L. Ji)

T.K. Zhao and X.L. Ji contribute equally to this work.

graphene aerogel structures which composed of dense interlined tubes and amorphous structure bearing quantities of dihedral angles could consume the incident waves through multiple reflection and scattering inside the 3D web structures. The interlinked ACNTs have both the virtues of amorphous CNTs (multiple reflection inside the wall) and crystaline CNTs (high conductivity), consuming the electromagnetic wave as resistance heat. ACNT/GA/BF composite has a good electromagnetic wave absorption performance.

Keywords: 3D graphene aerogel; ACNT networks; $BaFe_{12}O_{19}$; electromagnetic wave absorption property

1. Introduction

Recently, the electromagnetic wave pollution has attracted attention due to the development of electronic devices boosts the need for electromagnetic wave absorption materials with favorable properties. Generally, single material can hardly meet these requirements, such as lightweight, easy-preparation and strong-absorption in a wide frequency range **[1]**. The aforementioned problems can be solved by developing functional composite materials. More and more attention has been paid to the combination of magnetic and electric materials because of their adjustable electromagnetic performance and high coercivity which can be used in electromagnetic wave absorption **[2,3]**. Undoubtedly, new types of electromagnetic wave absorption composites are highly demanded to decrease the electromagnetic pollution and develop new microwave devices.

Hexagonal $BaFe_{12}O_{19}$ (BF) is widely used as magnetic substrate for electromagnetic wave absorption because of its high coercivity, excellent magnetization, easy preparation with low cost, and adjustable properties by controlling its morphology and particle size **[4-7]**. Especially, the extraordinarily high Curie temperature **[2]** ensures the thermostability of $BaFe_{12}O_{19}$. Yin et al. **[8]** reported that the $BaFe_{12}O_{19}$ nanoparticles and $BaFe_{12}O_{19}/Fe_3C$/carbon nanotube (CNT) composites obtained at 600□ performed good electromagnetic properties at low frequency. The substrate of $BaFe_{12}O_{19}$ can increase the end-use temperature of the composite material in a certain range.

Graphene has attracted wide attention as a new type of carbon material and potential

dielectric substrate in electromagnetic wave absorption field, which has excellent mechanical, thermal and electrical properties **[9,10]**. Due to the low-density, durable and excellent thermal-insulation properties, three dimensional (3D) graphene aerogel (GA) incorporated both the merits of graphene and aerogel is widely used as functional material for supercapactiors **[11,12]**, visible-light photocatalytics **[13-15]**, high-power lithium batteries **[16,17]** and biological adsorbent **[18,19]**, but rarely in electromagnetic wave absorption application. GA can be used for electromagnetic microwave absorption due to its porous and multi-layer microstructure, which constructs a 3D absorption system like foam sound absorption walls with low density, large specific surface area, and versatile electromagnetic properties.

Carbon nanotubes (CNTs), as an ideal electromagnetic wave absorber, have excellent broadband electromagnetic wave absorption performance. Their characteristics such as light weight, adjustable conductivity, high temperature anti-oxidation ability and good stability are attractive. CNTs have high specific surface area, small size, hollow and layered structures and high thermal and chemical stabilities **[20,21]**. Nevertheless, the expensive production costs of CNTs are inevitable for the requirement of high operating temperature, long synthesis period, complex processing steps, and catalyst support **[2]**. Hence, amorphous carbon nanotubes (ACNTs) have been widely utilized due to the less-stringent requirements and better electromagnetic properties. Our previous work **[22]** reported that the reflection loss (R) value of a lanthanum nitrate doped ACNT/Polyvinylchloride (PVC) composite was -25.02 dB at 14.44 GHz, and the frequency bandwidth corresponding to the reflector loss at -10 dB was up to 5.8 GHz within the frequency range of 2-18 GHz.

Herein, we first report the preparation of ACNT networks on a 3D graphene aerogel/ $BaFe_{12}O_{19}$ composite and its electromagnetic wave absorption property. This composite can achieve the multi reflection of electromagnetic wave with the foam structure in a 3D space and the high dielectric constant characteristics of graphene. Meanwhile, the $BaFe_{12}O_{19}$ with high permeability and the high coercivity can easily widen the absorption bandwidth and further expand the reflection loss as well as remedying the tremendous gap between low permeability and high complex permittivity of graphene. At the same time, the Curie temperature of the $BaFe_{12}O_{19}$ is so high that this composite can be realized in a certain range of free energy absorption. By using the high conductivity of ACNTs and the characteristics of the resistance heat are easy to produce,

it is possible to realize the electromagnetic wave energy loss.

2. Experimentals

The schematic diagram of fabrication process of ACNT/GA/BF nanocomposite is presented in Fig.1. The synthesis process includes three steps: first, BF was synthesized by self-propagating combustion using citric acid, $Fe(NO_3)_3$ and $Ba(NO_3)_3$ as precursor. Second, the obtained BF was mixed with GO solution and then treated with hydrothermal methods to prepare graphene/BF hydrogel. The obtained hydrogel was freeze-dried to obtain the graphene aerogel/BF composite. Last, the ACNTs were synthesized on the surface of the 3-D GA/BF composite by floating catalyst CVD method. The xylene was used as carbon source and ferrocene and silane were used as catalyst precursor. The detailed procedure was presented below.

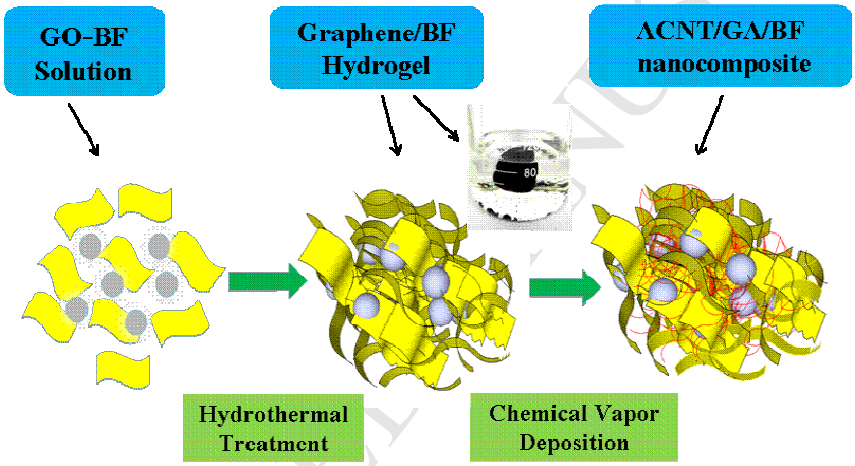

Fig. 1 Schematics of the fabrication process of ACNT/GA/BF composite

2.1 Synthesis of $BaFe_{12}O_{19}$ nanoparticles

The BF was synthesized by self-propagating combustion using citric acid complexed $Fe(NO_3)_3$ and $Ba(NO_3)_3$ as precursor and the mass ratio of $Fe(NO_3)_3$, $Ba(NO_3)_3$ and citric acid is 10:1:13. The ingredients were firstly dissolved into 50 ml distilled water and then ammonium hydroxide was added to adjust pH to 7. The obtained colloidal sol was dried at 120℃. The dried gel was heated at 400 ℃ until the self-propagating combustion process was triggered. After the combustion reaction, the powders were collected and cleaned by deionized water to get rid of the impurities for further application.

2.2 Fabrication of 3D graphene aerogel/BF composite

GO was obtained by a modified Hummers method **[23,24]**. Briefly, first the low temperature reaction stage, 1 g flake graphite and 1 g Na_2SO_3 mixed with 50 ml concentrated sulphuric acid

were stirred by magnetic stirring apparatus in ice water bath for 10 min. Then 6 g $KMnO_4$ was slowly put into the solution in order to reduce the heat influence caused by the redox reaction. The reaction was maintained at the temperature of about 0 □ for 1 h and the color of the solution was dark green in this step. And then followed by the middle temperature reaction stage, the beaker with the reactant was transferred to the water bath at 35□, stirring for 1 h. Finally, the high temperature reaction stage, the temperature of the water bath increased to 95 □ and meanwhile 80 ml distilled water was added to the solution slowly. The reaction time was 30 min in this stage. After the reaction, 200 ml distilled water was poured into the solution and added 6 ml H_2O_2 (volume ratio: 35%) through drop by drop. Some bubbles appeared in the solution and the color changed into luminous yellow. The resulting sample was washed until neutral by centrifugal machine and then dried at 40℃. As for the preparation of graphene/BF hydrogel, 0.1 g GO and 3 g BF were dispersed into 40 ml deionized water. Then 0.5 g tetraethyl orthosilicate (TEOS) was added into the solution through drop by drop in order to make SiO_2 coating promoting the growth of CNTs on the surface of graphene. The solution was treated by stirring and ultrasonic dispersion step by step each for 30 min. The solution became homogeneous and the color changed into yellow. The homogeneous solution was transferred to Teflon autoclave and treated at 140 ℃ for 12 h. After the reaction, 3D graphene/BF hydrogel was obtained. The hydrogel was treated with freeze-drying method (ALPHA 1-2/LD-2; -55 ℃ for 10 h) to obtain the aerogel. Finally, 3D graphene aerogel/BF composite was obtained.

2.3 Synthesis of ACNT networks on a GA/BF nanocomposite

The growth of ACNTs was similar with our previous work **[25]**, which performed by floating catalyst CVD in a quartz tube reactor (length 100 cm and diameter 60 mm). The reaction temperature was set at 770℃, and argon gas with a flow speed of 200 sccm was used as the carrier gas. The xylene, ferrocene and triethylsilane solution (the mole ratio of C: Fe: Si is 300: 10: 1) was used as carbon source and catalyst precursor which was injected into the reactor by a syringe pump at the speed of 0.3 ml/min. GA/BF composite was served as the substrate for the growth of ACNTs. After 30 min reaction, ACNT networks on a GA/BF composite were obtained inside the quartz tube.

2.4 Characterizations

The samples for transmission electron microscope (TEM, JEOL JEM-3100) were prepared

by ultrasonic vibration in ethanol (99.5%). The samples powder was directly used for field emission scanning electron microscope (FE-SEM, JEOL JSM-6700F and FEI Nova Nano SEM FEI 450). Cu K_α (λ=0.15406 nm) source was used for X-ray diffraction patterns (XRD, X'Pert PRO, PANalystal) at the scan rate of 4°/min. Raman scattering spectrum (λ=514 nm Ar laser, LabRAM HR800, HORIBA, spectral range: 200-2100 nm, resolution: 5 cm^{-1}, number of scans: 5) was carried out by using sample power. The as-obtained samples used for the characterization of electromagnetic wave absorption properties were prepared by mixing 30 wt.% ACNT/GA/BF (The weight ratio of the three components is about 0.4: 0.3: 9) composite with 70 wt.% molten paraffin, The ACNT/GA/BF nanocomposite films (the thickness is 2 mm) were prepared by a dip-coating method, then made into a doughnut-shaped sample (ϕ_{out}: 7.03 mm, ϕ_{in}: 3.00 mm). The complex permittivity (ε', ε'') and permeability (μ', μ'') components as the function of frequency of a sample are measured using a vector network analyzer (Agilent technologies E8362B; 10MHz-20GHz).

3. Results and discussion

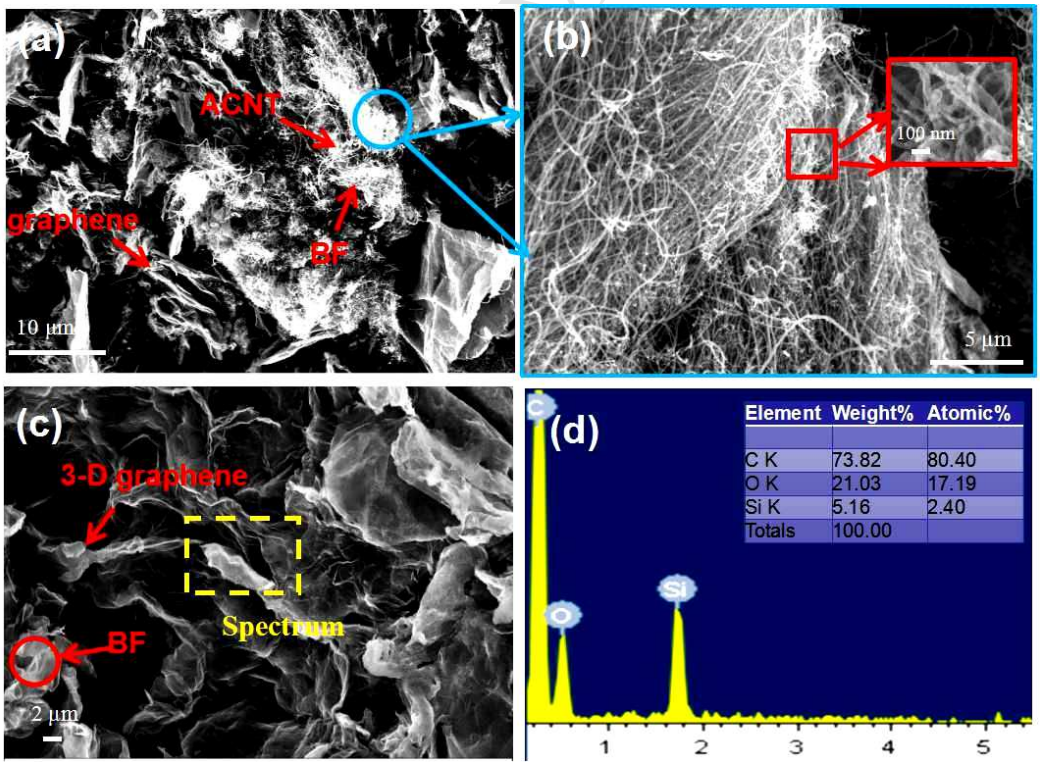

Fig. 2 SEM images of ACNT/GA/BF and GA/BF nanocomposites

(a) SEM image (low magnification) of ACNT/GA/BF nanocomposite, (b) a magnified image of the composite for ACNTs and catalyst particles encapsulated by carbon (inset), (c) SEM image of GA/BF composite,

and (d) EDS result for a selected area of (c), where graphene is coated with SiO_2

Fig. 2 shows SEM images of ACNT/GA/BF and GA/BF nanocomposites. Fig. 2(a) shows the 3D structure of ACNT/GA/BF nanocomposite. The BF nanoparticles disperse homogeneously among the porous graphene structures. ACNT networks with high growth density are synthesized on the surface of BF and graphene. Fig. 2(b) is an enlarged figure of the circled zone in Fig. 2(a). Aligned ACNTs can be seen in this picture. There exists carbon particles adhered with the tubes wall, inactivating the catalyst and forming the sphere shape. SEM image of the carbon sphere is shown in the top-right corner of Fig. 2(b). The carbon sphere intertwined with CNTs can be seen clearly. Fig. 2(c) is the 3D graphene/BF composite before the growth of ACNTs and the 3D structure can also be observed inside or on the surface of the graphene. The composite is coated with SiO_2 which is formed during the hydrothermal process of TEOS. The SiO_2 coating can promote the growth of ACNTs because the combination bond between iron catalyst and SiO_2 is stronger than that of graphene. Fig. 2(d) is the EDS result of the rectangular part of Fig. 2(c). The existence of Si and O elements in the spectrum proves the formation of SiO_2 coating.

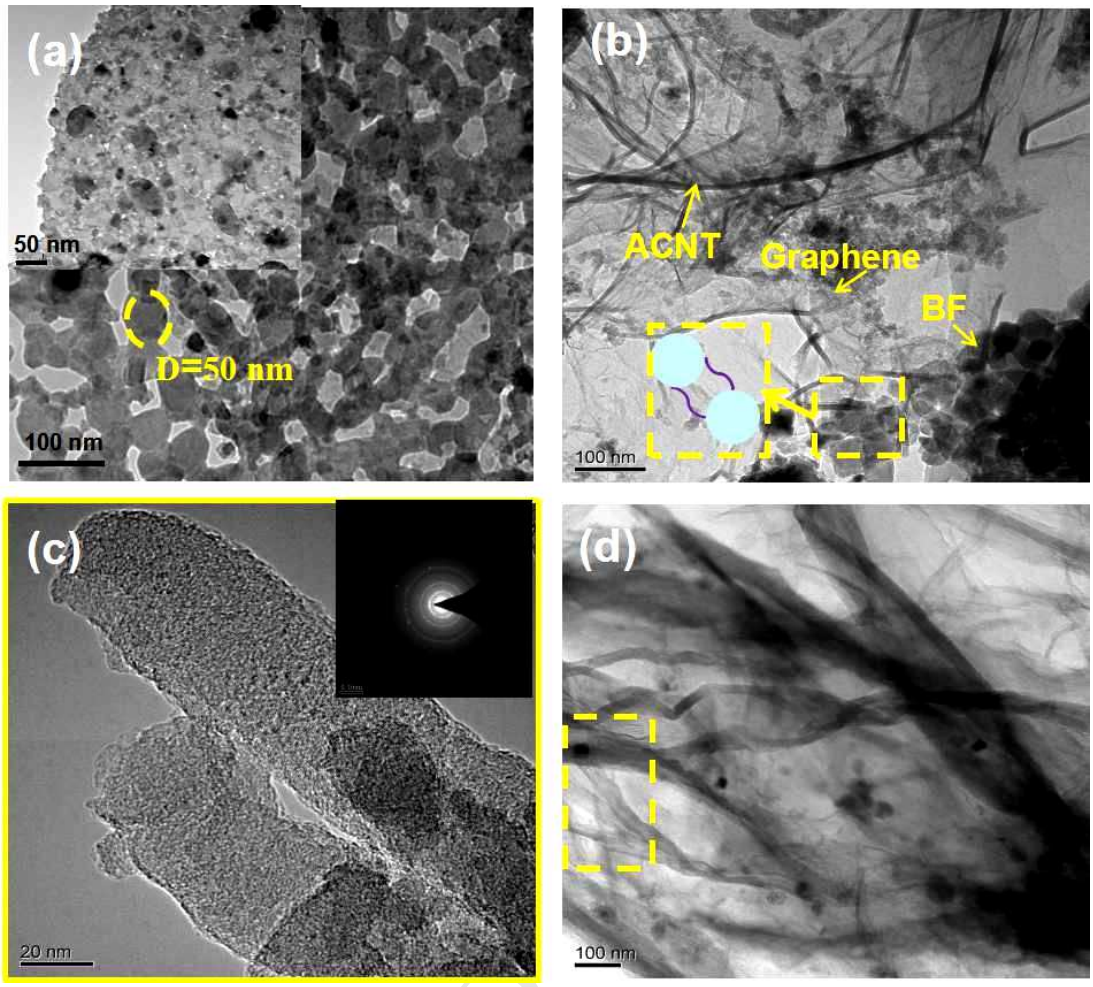

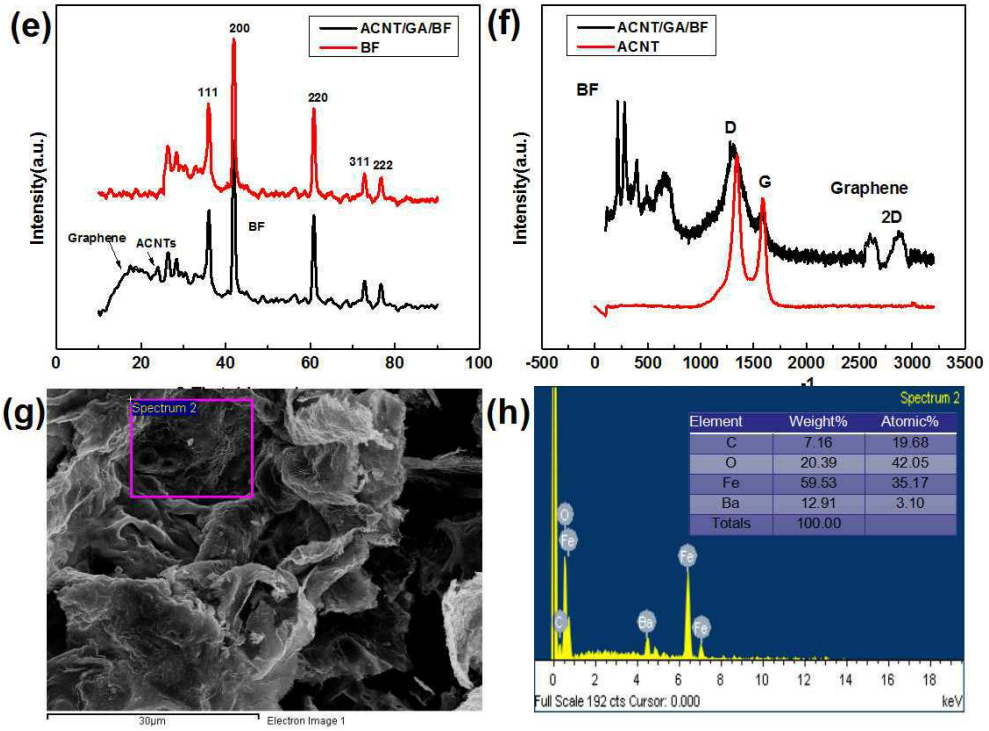

Fig. 3 Morphology and structure analysis of ACNT/GA/BF nanocomposite

(a) TEM image of BF; (b) TEM image of ACNT/GA/BF composite; the schematic plot shows the interlinked BF/ACNT structure. (c)(d) TEM images of the interlinked ACNT/graphene structure and enlarged picture of ACNT. The schematic plot shows the interlinked graphene/ACNT structure. (e) XRD spectra of ACNT/GA/BF and BF; (f) Raman spectra of ACNT/GA/BF and ACNTs; (g) and (h) EDS spectrum of BF

Fig. 3 is the morphology and structure of ACNT/GA/BF nanocomposites. The top-left corner of Fig. 3(a) shows the morphology of $BaFe_{12}O_{19}$ nanoparticles synthesized by self-propagating combustion. These nanoparticles, with average particle size of about 50 nm, combine and interlink with each other forming net structures (in the inserted image). Fig. 3(a) shows that there exist some pores between the BF (in the inserted image). The pores as well as the net structures of these nanoparticles explain well the reason why the density of the BF is far lighter than that of other $BaFe_{12}O_{19}$ materials and the reason why there exists significant volume expansion during the

self-propagating combustion. Fig. 3(b) is the TEM images of ACNT/GA/BF nanocomposites. The BF in the bottom-right corner shows the same nanoparticle morphology compared to Fig. 3(a). The schematic plot in Fig. 3(b) shows the interlinked structure of ACNT and BF. Fig. 3(c) and Fig. 3(d) are TEM images of the enlarged pictures of ACNTs and interlinked ACNT/graphene structures respectively. The schematic plot enclosed in Fig. 3(d) shows the interlinked graphene/ACNT structures. Fig. 3(c) shows the carbon clusters and small graphene sheets are lined in random positions within long-distance range, indicating the amorphous structures. The diffraction rings of the selected area electron diffraction (SAED) also show the existence of amorphous structure. From Figs. 3(a)-(d), it can be concluded that the ACNTs form into networks connecting BF and graphene together so as to increase the structure stability and the conductivity for the electromagnetic wave absorption properties. Fig. 3(e) is XRD spectra of ACNT/GA/BF and BF. The BF peaks in the two curves are mainly coincident, indicating that the structure of BF doesn't change too much during the synthesis procedure. The best strong peak of BF is at around 40°. The spectrum of the ACNT/GA/BF shows both the carbon peak causing by graphene/ACNT (at around 20°) and BF peaks. The BF spectrum has sharp peaks showing the good crystallinity. Fig. 3(f) is Raman spectra of ACNT/GA/BF and ACNTs. Both of the spectra have two obvious peaks centered at 1324.7 and 1593.2 cm^{-1}, namely D and G modes of CNTs. The D peak at 1324.7 cm^{-1} stems from a symmetry-lowering effect due to the defects of nanotube and amorphous structures. The G peak at 1593.2 cm^{-1} indicates the graphite crystallinity of this carbon material. The G peak not only stems from graphene but also a result of the combined effect of ACNTs and graphene. The ratio of I_D to I_G is used to characterize the structure integrity of carbon materials. The ACNT samples have a relative high ratio of I_D/I_G =1.387 showing that there exist large

amounts of defects in the tube-wall structures. The ACNT/GA/BF samples show both the characteristic peak of BF (labeled in the image) and graphene/ACNTs. The presence of 2D peak proves the existence of graphene. Figs. 3(g, h) are the EDS spectrum of BF. The ratio of Ba to Fe element is about 1:12, which proves the existence of $BaFe_{12}O_{19}$.

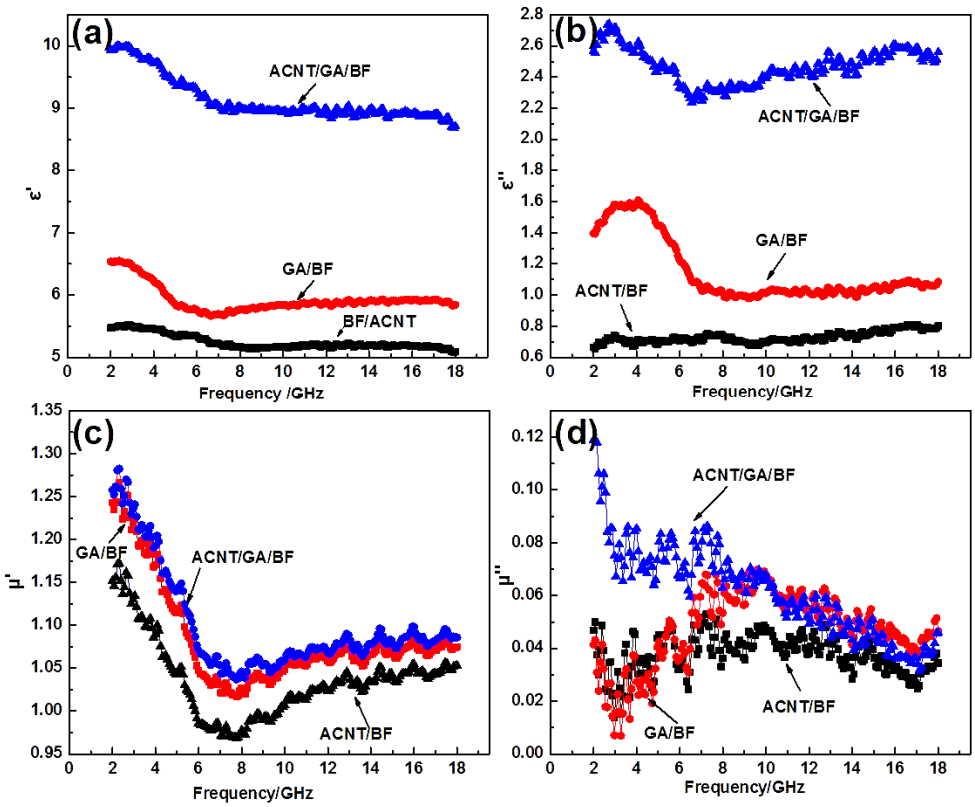

Fig. 4 Complex permittivity (ε', ε'') (a, b) and permeability (μ', μ'') (c, d) spectra of ACNT/GA/BF, GA/BF and ACNT/BF composites *vs* frequency.

The complex permittivity (ε', ε'') and permeability (μ', μ'') spectra of ACNT/GA/BF, GA/BF and ACNT/BF composites *vs* frequency are shown in Figs. 4(a)-(d). The permittivity and permeability are used for characterization of dielectric constant and magnetic loss properties of the electromagnetic wave absorption materials. In Figs. 4(a, b), the dielectric constant (ε') decreases slightly with frequency increasing, which is a normal behavior and is also observed by other researchers **[10]**. According to Koops theory based on the Maxwelle Wagner model for the inhomogeneous double layer dielectric structures **[8]**, the well conducting grains in ferrous crystal

are separated by poorly conducting grain boundaries. Here, in the formation of grain boundaries, the interaction between $BaFe_{12}O_{19}$ and CNTs or graphene sheets plays an important role. At low frequencies, the grain boundaries are more effective than the conducting grains. Due to the high resistance of the grain boundaries, the hopping electrons will pile up and produce polarization at these areas. The electronic conduction is high at low frequencies due to the polarization. However, the electron exchange between Fe^{3+} and Fe^{2+} ions cannot follow the fast alternating field, which decreases the probability of electrons reaching the grain boundaries and the interfacial polarization **[9, 13]**. In Figs. 4(a, b), the dielectric constant (ε') and dielectric loss (ε'') of GA/BF is lower than that of ACNT/GA/BF nanocomposite, which might be due to the growth of ACNT networks increasing the conductivity of the composites. The interlinked ACNT networks as well as Fe catalyst particles inside the tubes increase the conductivity, which makes ACNT networks possess both the advantages of amorphous structure (the small graphite clusters inside the tube-wall can cause the scattering and increase the path length) and crystal structure (good conductivity). ACNT networks & BF structures have a better dielectric polarization and relaxation effects despite the poor conductivity of amorphous structure. When the conductive phase is distributed in the insulating matrix to form composite materials, the free charge gathering will exist in the insulation/conductor interface due to the difference in the two phase conductive performance. The high tube density and the interlinked structure of ACNT networks may increase the probability for the tubes to overlap and twine each other for forming conductive networks interlinked with $BaFe_{12}O_{19}$ to improve the dielectric polarization properties. Besides, the interlinked ACNT/GA/BF structure may also benefit the dielectric polarization properties and the high length-diameter ratio of CNTs is also beneficial to the conductivity and the dielectric loss. It is also noted that the dielectric constant (ε') and dielectric loss (ε'') of 3D GA/BF composite is lower than that of ACNT/BF composite, which might be due to that graphene have more connected surface area and higher conductivity after the annealing process at 750 □ than that of ACNTs. In Figs. 4(c, d), it is worth noting that a minimum value as well as a maximum value are observed for μ' and μ'', respectively, those obvious peaks for μ' and μ'' can be ascribed to a resonance phenomenon, which is also showed in Fig. 5(b). The tendency of the lines in Figs. 4(c, d) is similar, because carbon nanomaterials have poor magnetic loss and the several lines are all reveal the properties of $BaFe_{12}O_{19}$.

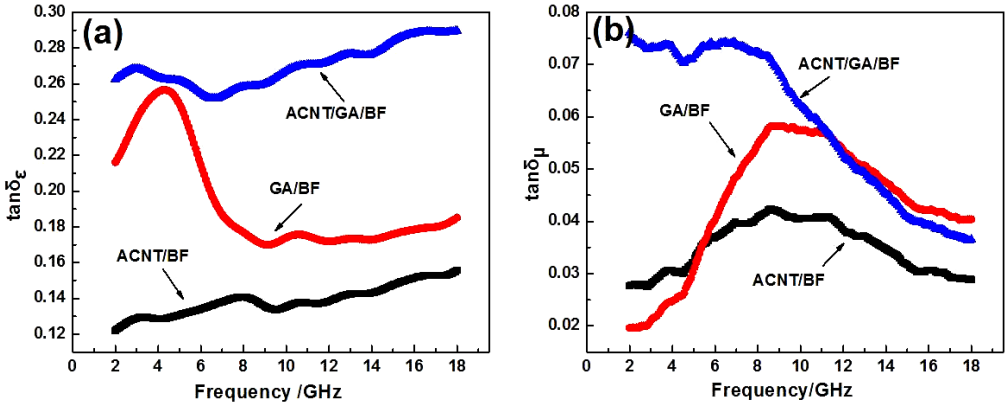

Fig. 5 Dielectric loss tangent ($tan\delta_{\varepsilon}$) (a) and magnetic loss tangent ($tan\delta_{\mu}$) (b) of ACNT/GA/BF, GA/BF and ACNT/BF composites *vs* frequency

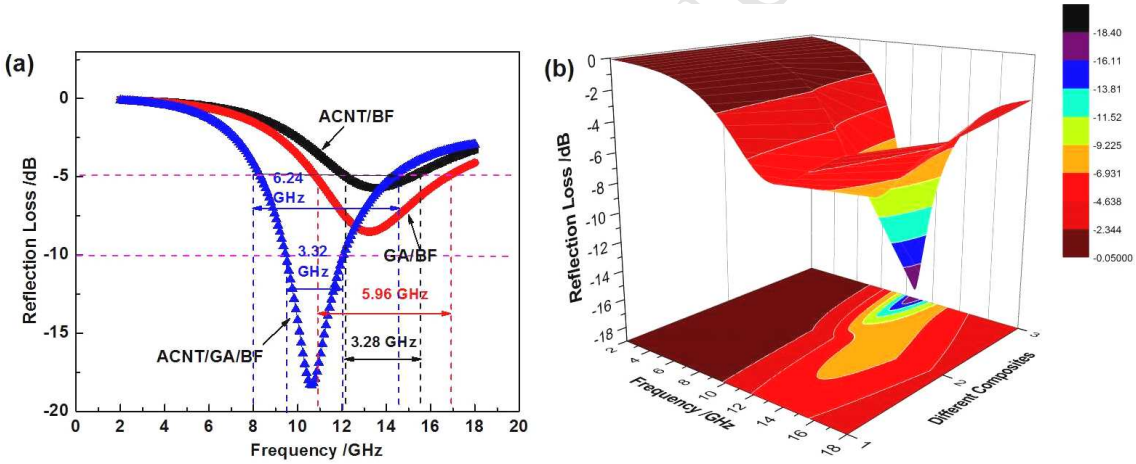

Fig. 6 (a) Reflection loss of ACNT/GA/BF, GA/BF and ACNT/BF composites with a thickness of 2.0 mm in the frequency range of 2-18 GHz. (b) Three-dimensional presentations of the reflection loss of ACNT/GA/BF, GA/BF and ACNT/BF composites. Here 1, 2 and 3 in Y axis represent ACNT/BF, GA/BF and ACNT/GA/BF respectively.

$$R(dB) = 20\log_{10}\left|\frac{Z_{in}-1}{Z_{in}+1}\right| \tag{1}$$

$$Z_{in} = \left(\frac{\mu_r}{\varepsilon_r}\right)^{\frac{1}{2}} \tanh\left[j\left(\frac{2\pi fd}{c}\right)(\mu_r\varepsilon_r)^{\frac{1}{2}}\right] \tag{2}$$

where Z_{in} is the normalized input impedance at free space and material interface, $\varepsilon_r=\varepsilon'- j\varepsilon''$ is the complex permittivity, and $\mu_r= \mu'-j\mu''$ is the complex permeability of absorbers, f is the frequency of the microwave in free space, d is the thickness of the absorber, and c is the velocity of light in free space. The impedance matching condition is given by $Z_{in}=1$ to represent the perfect absorption properties. The surface reflectivity of an absorber was presented by a function including six parameters of ε', ε'', μ', μ'', f and d **[26,27]**. Thus, if the six parameters are known, the absorption properties of the material can be calculated. The values of reflection loss in Fig. 6 (a, b) were calculated using Eqs. (1) and (2) with the measured values of ε', ε'', μ', μ'', f and d (see Fig. 4). Fig. 6(b) is three-dimensional presentations of the reflection loss of ACNT/GA/BF, GA/BF and ACNT/BF nanocomposites. In the frequency range of 2-18 GHz, the minimum absorption peak of ACNT/GA/BF nanocomposites with a thickness of 2 mm is -18.35 dB at 10.64 GHz. The frequency bandwidth of the reflection loss below -10 dB and -5 dB is 3.32 and 6.24 GHz, respectively. For contrast, under the same matching thickness (d_m=2.0 mm), the absorption peaks of ACNT/GA/BF and ACNT/BF becomes more flat and wide, The minimum absorption peak of GA/BF composite is about -8.52 dB at 13.28 GHz, the frequency bandwidth of the reflection loss below -5 dB is 5.96 GHz. The minimum absorption peak of ACNT/BF composite is about -5.69 dB at 13.12 GHz, the frequency bandwidth of the reflection loss below -5 dB is 3.28 GHz. It can also be proved through Fig. 5 (a) that the dielectric loss tangent ($\tan\delta_\varepsilon$) of ACNT/GA/BF is much higher than that of the GA/BF as well as ACNT/BF. The electromagnetic wave absorption mechanism of ACNT/GA/BF nanocomposites is depicted in Fig. 7. The good electromagnetic wave absorption properties of the 3D GA/ACNT network structures may be explained by the following several reasons. First, the network structures with high density interlinked tubes were

formed conductive networks to connect 3D GA, leading to more physical contacts between conductive graphene sheets, therefore increasing the resonance circuit density, which is consistent with the electrical conductivity rising and larger dielectric loss tangent. The tubes possess excellent electrical conductivity and high aspect ratios. The conducting networks would interact and attenuate the electromagnetic radiation in the absorbers effectively. Second, it exist the polarization relaxation of defects or π-electron and interfacial polarization between graphene and BF.

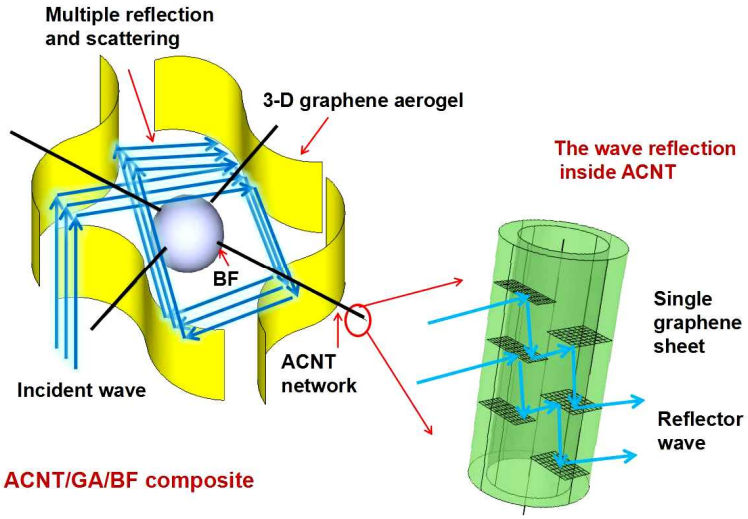

Fig. 7 Electromagnetic wave absorption mechanism schematics of ACNT/GA/BF nanocomposite

The 3D graphene foam structure with dense interlinked tubes and the special structure of ACNTs with quantities of dihedral angles can consume the incident waves through multiple reflection and scattering inside the foam structures. The dihedral angles could be easily formed within the graphene sheet stacks of ACNT tube-walls, which cause multiple reflections of electromagnetic wave, prolonging the propagation path of electromagnetic waves in the absorbers **[22]**. The multiple reflections of electromagnetic wave lead to the larger losses of electromagnetic energy. Furthermore, the intricate foam structures are consisting of interlinked ACNTs and entangled

conductive graphene sheets spontaneously and intensely response to the broadband incident wave, presenting as tremendous resistance-inductance-capacitance coupled circuits. The interaction of electromagnetic waves with dielectric materials intensified the molecular motions such as ionic conduction, dipolar polarization relaxation, etc., leading to energy dissipation in the form of heat through molecular friction and dielectric loss and the highly conductive networks would also consume the electromagnetic wave as resistance heat.

4. Conclusions

ACNT/GA/BF nanocomposite was synthesized by floating catalyst CVD using BF nanoparticles (self-propagating combustion method) and GO as raw materials. ACNTs were synthesized on the surface of the 3-D GA/BF composite by floating catalyst CVD. The minimum absorption peak of ACNT/GA/BF nanocomposites is -18.35 dB at 10.64 GHz in the frequency range of 2-18 GHz. The frequency bandwidth below -10 dB is 3.32 GHz. The special 3D graphene foam structure with dense interlinked tubes forming the conducting network and the special structure of ACNTs with quantities of dihedral angles can consume the incident waves through multiple reflection and scattering inside the foam structures.

Acknowledgments

This work was supported by the Natural Science Foundation of China (51572221, 51672221), the China Aeronautical Science Fund (2014ZF53074), the Natural Science Foundation of Shaanxi Province (2016JQ5108) and the Graduate Innovation Seed Fund of Northwestern Polytechnical University (Z20160011).

References

[1] Y. Ding, L. Zhang, Q.L. Liao, G.J. Zhang, S. Liu, Y. Zhang, Electromagnetic wave absorption in reduced graphene oxide functionalized with Fe_3O_4/Fe nanorings, Nano Res. 9 (2016) 2018-2025.

[2] M.J. Liu, X.L. Liu, J.X. Wang, Z.X. Wei, L. Jiang, Electromagnetic synergetic actuators based on polypyrrole/Fe_3O_4 hybrid nanotube arrays, Nano Res. 3 (2010) 670-675.

[3] K.H. Tan, R. Ahmad, M.R. Johan, Electromagnetic and microwave absorbing properties of amorphous carbon nanotube-cadmium selenide quantum dot hybrids, Mater. Chem. Phys. 139 (2013) 66-72.

[4] A. Ohlan, K. Singh, A. Chandra, S.K. Dhawan, Microwave absorption behavior of core-shell structured poly(3,4-ethylenedioxy thiophene)-barium ferrite nanocomposites, ACS Appl. Mater. Interfaces 2 (2010) 927-933.

[5] S.G. Kim, W.N. Wang, T. Iwaki, A.A> Yabuki, K. Okuyama, Low-temperature crystallization of barium ferrite nanoparticles by a sodium citrate-aided synthetic process, J. Phys. Chem. C 111 (2007) 10175-10180.

[6] L.C. Li, K.Y. Chen, H. Liu, G.X. Tong, H.S. Qian, B. Hao, Attractive microwave-absorbing properties of M-$BaFe_{12}O_{19}$, ferrite, J. Alloys Compd. 557 (2013) 11-17.

[7] T.H. Ting, K.H. Wu, Synthesis, characterization of polyaniline/$BaFe_{12}O_{19}$, composites with microwave-absorbing properties, J. Magn. Magn. Mater. 322 (2010) 2160-2166.

[8] L.J. Yin, T. Chen, S.Y. Liu, Y.Q. Gao, B. Wu, Y.F. Wei, G. Li, X. Jian, X. Zhang, Preparation and microwave-absorbing property of $BaFe_{12}O_{19}$ nanoparticles and $BaFe_{12}O_{19}$/Fe_3C/CNTs composites, RSC Adv. 5 (2015) 91665- 91669.

[9] H. Wang, H.H. Gao, M.X. Chen, X.Y. Xu, X.F. Wang, C. Pan, J.P. Gao, Microwave-assisted

synthesis of reduced graphene oxide/titania nanocomposites as an adsorbent for methylene blue adsorption, Appl. Surf. Sci. 360 (2015) 840-848.

[10] X.Q. Meng, J. Deng, J.W. Zhu, H.P. Bi, E.J. Kan, X. Wang, Cobalt sulfide/graphene composite hydrogel as electrode for high-performance pseudocapacitors, Sci. Rep. 6 (2016) 21717.

[11] S. Ye, J. Feng, Self-assembled three-dimensional hierarchical graphene/polypyrrole nanotube hybrid aerogel and its application for supercapacitors, ACS Appl. Mater. Interfaces 6 (2014) 9671-9679.

[12] H.L. Wang, C.M.B. Holt, Z. Li, X.H. Tan, B.S. Amirkhiz, Z.W. Xu, B.C. Olsen, T. Stephenson, D. Mitlin, Graphene-nickel cobaltite nanocomposite asymmetrical supercapacitor with commercial level mass loading, Nano Res. 5 (2012) 605-617.

[13] W.J. Han, L. Ren, L.J. Gong, X. Qi, Y.D. Liu, L.W. Yang, X.L. Wei, J.X. Zhong, Self-assembled three-dimensional graphene-based aerogel with embedded multifarious functional nanoparticles and its excellent photoelectrochemical activities, ACS Sustain. Chem. Eng. 2 (2014) 2189-2196.

[14] Z.W. Tong, D. Yang, J.F. Shi, Y.H. Nan, Y.Y. Sun, Z.Y. Jiang, Three-dimensional porous aerogel constructed by g-C_3N_4 and graphene oxide nanosheets with excellent visible-light photocatalytic performance, ACS Appl. Mater. Interfaces 7 (2015) 25693-25701.

[15] L. Chen, R. Du, J.H. Zhu, Y.Y. Mao, C. Xue, N. Zhang, Y.L. Hou, J. Zhang, T. Yi, Three-dimensional nitrogen-doped graphene nanoribbons aerogel as a highly efficient catalyst for the oxygen reduction reaction, Small 11 (2014) 1423-1429.

[16] X. Yao, G.L. Guo, X. Ma, Y. Zhao, C.Y. Ang, Z. Luo, K.T. Nguyen, P.Z. Li, Q.Y. Yan, Y.L.

Zhao, In situ integration of anisotropic SnO_2 heterostructures inside three-dimensional graphene aerogel for enhanced lithium storage, ACS Appl. Mater. Interfaces 7 (2015) 26085-26093.

[17] B. Wang, W.A. Abdulla, D. Wang, X.S. Zhao, A three-dimensional porous $LiFePO_4$ cathode material modified with a nitrogen-doped graphene aerogel for high-power lithium ion batteries, Energ. Environ. Sci. 8 (2015) 869-875.

[18] S. Mahpishanian, H. Sereshti, Three-dimensional graphene aerogel-supported iron oxide nanoparticles as an efficient adsorbent for magnetic solid phase extraction of organophosphorus pesticide residues in fruit juices followed by gas chromatographic determination, J. Chromatogr. A 1443 (2016) 43-53.

[19] Y. Zhuang, F. Yu, J. Ma, J.H. Chen, Facile synthesis of three-dimensional graphene-soy protein aerogel composites for tetracycline adsorption, Desalin. Water Treat. 57 (2015) 1-10.

[20] O. Duman, S. Tunc, B.K. Bozoglan, T.G. Polat, Removal of triphenylmethane and reactive azo dyes from aqueous solution by magnetic carbon nanotube-k-carrageenan-Fe_3O_4 nanocomposite, J. Alloys. Compd. 687 (2016) 370-383.

[21] O. Duman, S. Tunc, T.G. Polat, B.K. Bozoglan, Synthesis of magnetic oxidized multiwalled carbon nanotube-k-carrageenan-Fe_3O_4 nanocomposite adsorbent and its application in cationic Methylene Blue dye adsorption, Carbohydr. Polym. 147 (2016) 79-88.

[22] T.K. Zhao, C.L. Hou, H.Y. Zhang, R.X. Zhu, S.F. She, J.G. Wang, T.H. Li, Z.F. Liu, B.Q. Wei, Electromagnetic wave absorbing properties of amorphous carbon nanotubes, Sci. Rep. 4 (2014) 5619.

[23] J. Chen, B. Yao, C. Li, G. Shi, An improved Hummers method for eco-friendly synthesis of

graphene oxide, Carbon 64 (2013) 225-229.

[24] J. Chen, Y. Li, L. Huang, C. Li, G. Shi, High-yield preparation of graphene oxide from small graphite flakes via an improved Hummers method with a simple purification process, Carbon 81 (2015) 826-834.

[25] T.K. Zhao, X.L. Ji, H.Z. Liu, P.Y. Rao, W.J. Liu, C.Y. Xiong, T.X. Li, C. Wang, Growth of well-aligned carbon nanotubes with different shapes, Appl. Surf. Sci. 357 (2015) 2136-2140.

[26] C.L. Hou, T.H. Li, T.K. Zhao, W.J. Zhang, Y.L. Cheng, Electromagnetic wave absorbing properties of carbon nanotubes doped rare metal/pure carbon nanotubes double-layer polymer composites, Mater. Design 33 (2012) 413-418.

[27] C.L. Hou, T.H. Li, T.K. Zhao, H.G. Liu, L.H. Liu, W.J. Zhang, Electromagnetic wave absorbing properties of multi-wall carbon nanotube/Fe_3O_4, hybrid materials, New Carbon Mater. 28 (2013) 184-190.

- BNR was prepared by a self-propagating combustion process.
- ACNT networks have been synthesized using CVD.
- The ACNT/GA/BNR composite has 3D network structure.